Impact of Adversarial Examples on the Efficiency of Interpretation and Use of Information from High-Tech Medical Images

Aleksandra Vatian, Natalia Gusarova, Natalia Dobrenko, Sergey Dudorov, Niyaz Nigmatullin,
Anatoly Shalyto, Artem Lobantsev
ITMO University
Sankt-Petersburg, Russia
alexvatyan@gmail.com

Abstract—**In this paper we discuss the possibility of adversarial examples appearance in high-tech medical images (Computer tomography and Magnetic resonance imaging), due to the noise inherent in the technology of their formation, and therefore we suggest ways to counteract this effect. As the idea of the paper we put two questions: 1.Can individual instances of real high-tech medical images work as AE when being analyzed with the use of neural networks? 2. Is it possible to defend oneself against such «natural» adversarial attacks with the simplest possible means? In our research, we tried the following defence methods: adversarial training, Gaussian data augmentation and bounded RELU (see section 3 for a detailed description). We conducted the experiment with the use of the neural network - a variant of convolutional network structure combining U-Net with the region proposal networks. As the source data two datasets were chosen - the Lung Image Database Consortium image collection containing 1018 lung cancer screening thoracic CT scans and Brain MRI DataSet containing clinical imaging data of glioma patients (a total of 274 cases). The experiments showed that the degree of manifestation of AE varies depending on the type of training model. When training a model not using techniques of defences on adversarial examples, the number of incorrectly recognized images is quite large (200 per 10,000 for CT and 285 per 10,000 for MRI). By proper selecting of the activation function of CNN, it can be reduced to 60 and 68, respectively. With augmentation of training dataset by Gaussian noised images, this number drops to 21 and 26. An even greater reduction in the number of incorrectly recognized images is achieved using the Adversarial Training method – 12 and 15. Thus, it is shown that the adversarial effect is possible after the application of adversarial training techniques, but the degree of noise in such an image will be much higher than before using these techniques, and it will be easy enough for the doctor to recognize them visually and exclude them from further consideration.**

I. Introduction

In recent years, medical images have entered the category of leading diagnostic tools. High-tech medical images, such as formed by computer tomography (CT) or Magnetic resonance imaging (MRI), have become part of the daily practice of doctors. For example, medical images are considered one of the most informative means of diagnosing serious diseases such as lung cancer, brain cancer, multiple sclerosis.

However, the accuracy of diagnosis of these diseases, even with the use of high-tech medical images, leaves much to be desired. For example, the accuracy of diagnosing lung cancer even by an experienced radiologist does not exceed 75% with a high sensitivity and rather low specificity [1]. The fact is that the difference between malignant and benign pulmonary nodes lies mainly in their morphological characteristics, which are poorly described by a set of independent features and are to be evaluated integrally. Therefore, in recent years, the attention of both physicians and IT professionals has been drawn to the development of automated tools for diagnosing cancer.

One of the most promising approaches was the use of neural networks, which do not require the assignment of classifying features in an explicit form. In this direction great efforts were made by the developers: for example, the Kaggle's Data Science Bowl 2017 competition [2] was entirely devoted to the diagnosis of lung cancer. Neural networks of various types were used, including convolution neural networks (CNN), deep neural network (DNN), stacked autoencoder (SAE) neural network etc. [3]. Diagnostic accuracy on experimental datasets exceeded 90% [4, 5].The components are arranged in the order in which they should be in the article.

However, in 2014, the phenomenon of adversarial examples (AE) was discovered [6], which significantly undermined the credibility of the results obtained by neural networks. According to [6], "adversarial examples are obtained by imperceptibly small perturbations to a correctly classified input image, so that it is no longer classified correctly".

In subsequent studies [7], it was shown that it is quite easy to create AE that are difficult to distinguish visually, since they are similar to the result of noise on benign images. Such examples were built for images from various subject areas, including medical images [8].

However, the appearance of AE is mainly associated with attacks of adversaries (intruders); other ways of the appearance of AE in images, including medical images, are not considered in the available literature. This paper discusses the possibility of an appearance of AE in high-tech medical images, due to the noise inherent in the technology of their formation, and suggests ways to counteract this effect.

II. Background and Related Works

A. Nature of Adversarial Examples

The phenomenon of AE occurs when processing images using neural networks. In the notion of [9], a full neural network $F(x)$ is defined as follows:

$$F(x) = \text{softmax}(Z(x)) = y \quad (1)$$

consisting of layers

$$F = \text{softmax} \circ F_n \circ F_{n-1} \circ \ldots \circ F_1 \quad (2)$$

where

$$F_i(x) = \sigma\left(\theta_i \cdot x\right) + \hat{\theta}_i . \quad (3)$$

Here $x \in R^n$ is an input vector, $y \in R^m$ is an output vector, σ is some non-linear activation function, θ_i is a matrix of model weights, and $\hat{\theta}_i$ is a vector of model biases. Note that the output vector y is formed using softmax function $Z(x) = z$ so that $0 \le y_i \le 1$ and $y_1 + \ldots + y_m = 1$, y_i being the probability that input x belongs to class i. In this case, the entire network works as a classifier giving the label $C(x) = \arg\max_i F(x)_i$ to the input x. The correct label of x is denoted as $C^*(x)$.

[6] defines AE in a following way: it is an input x' similar to a valid input x so that $C(x') \neq C^*(x)$. A closeness (similarity) between x' and x is, as a rule, associated with the visual indistinguishability of the corresponding images x' and x and should be defined in a proper way. Most widely-used are three distance metrics: L_0 (the number of differing pixels in x' and x); L_2 (the standard Euclidean distance between x' and x); L_∞ (the maximum difference between any pair of pixels in x' and x). However, the generally accepted metric for measurement of human perceptual similarity has not yet been developed.

Techniques of artificial AE formation are called adversarial attacks. In our work we use the attacks of two simplest types: fast gradient sign method (FGSM) [10] and Jacobian-based saliency map approach (JSMA) [11]. In FGSM adversarial example is generated by performing one step in the direction of the gradients sign with step-width ε as hyper-parameter. JSMA estimates the Jacobian values of target and not-target classes and thus chooses pixel of input image to be perturbed.

B. Adversarial Examples in High-Tech Medical Images: State of the Art

Analysis of the literature shows that the study of the effect of AE on medical images mainly focuses on target attacks. These attacks aim to make the neural network to classify an adversarial input x' as a given target class t such that $t \neq C^*(x)$ although x' and x are visually similar. Two types of problems are mainly under consideration: on the one hand, the potential hazards of adversarial attacks; on the other hand, the ways to artificially construct targeted adversarial examples and to counteract them.

Namely, the authors [12] highlight economic and organizational features of the healthcare system that favor adversarial attacks as a means of conscious fraud. Scenarios for deception of health insurance companies with application of AE in dermatology, radiology and ophthalmology are discussed. In order to show the vulnerability of standard medical deep learning systems to adversarial attacks, the authors implement patch [13] and human-imperceptible attacks. They argue that the white and black box projected gradient descent (PGD) attack strategies [14] are the best for the latter case, that is, attacks trained using PGD are minimally visible.

In [15], the authors apply to chest X-Ray images AE attacks of different categories, namely: gradient-based attacks, score-based attacks and decision-based attacks [16]. In the latter case, the attack relies on the final decision of the model and manifests itself in a blurring of the classification boundary. The authors [15] apply methods like Gaussian blur, contrast reduction and additive Gaussian noise and show that in all these cases, the result of the attack is visually noticeable in the image.

Authors [17] examined the robustness of a variety of medical imaging models in relation to various disturbances, including AE as well as noise, outliers and ambiguous input data. Dermatoscopic images and whole brain MRI scans were used as the originals, and different variants of gradient-based adversarial example generation method [10], [18] were applied. To simulate noisy images modality-specific distributions were used, namely: Gaussian noise for dermatoscopic images and Rician noise for brain MRI images. The authors have visually shown that all the above types of added perturbations are effectively imperceptible to the human eye, and moreover, the manifestation of AE in the image can be considered as a kind of noise. For a comparative study of the statistical properties of the above kinds of typical noise vs adversarial noise, the authors used to-distributed Stochastic Neighbor Embedding [19].

At the same time, another type of AE attacks, namely untargeted adversarial attack, is defined in [6]. In this case, the AE can be any input x' such that $C(x') \neq C^*(x)$ provided that x and x' are close (similar) in a proper way. With regard to medical images it means that the valid and adversarial images should be indistinguishable under conditions typical for their formation. The review showed that the possibility of an untargeted adversarial attack on medical images as well as means to combat it are hardly considered in the literature.

C. Noise Characteristics in High-Tech Medical Images

As a rule, AE are being masked as adding noise components to the valid image. In this paper, the problem of AE is considered on two examples of high-tech medical images – namely on CT images of the lungs as well as on MRI images of brain.

Noises of high-tech medical images can be characterized by various parameters, but the most wide-spread are the type of statistical distribution and peak signal-to-noise ratio (*PSNR*):

$$PSNR = 20 \log_{10}\left(\frac{MAX_i}{\sqrt{MSE}}\right). \quad (4)$$

Here MAX_i is the maximum brightness of an image pixel,

MSE is the mean square error of pixels within the whole image. It should be noted that in various sources the value of *PSNR* is given either in decibels or directly in relative units, which complicates the comparative analysis.

Various ways of noise reduction of high-tech medical images are proposed [20], however, radiologists' opinion of them is contradictory [21], since noise suppression measures may impair the distinctiveness of the image. In this regard, physicians prefer not to use noise reduction during visual inspection, and most of the problems are solved by radiologists directly in the presence of noise. Moreover, in recent years, low-dose CT has been increasingly used in clinical practice [22], which is more benign to the patient's health, but leads to a significant increase in the noise level in the image.

Noises on CT images have complex nature, depending on the equipment parameters (first of all, tube current-time product being the product of the x-ray tube current and the CT scanner exposure) as well as on the patient parameters (for example, his size) and on the experiment parameters (for example, slice thickness) []. As shown in the literature (see [24] and the review in it), the CT noise statistics is characterized by a non-stationary spatial distribution and the presence of higher moments. It is modeled differently in different spatial areas of the image. A mixture of off-center gamma distributions (nc-Γ) is proposed as the most generalized model. Other sources use special versions of this model up to the Gaussian distribution. The working range of *PSNR* for CT images lies in the range of 30–40 dB, and for low-dose CT it decreases to 20–30 dB and below [22, 25, 26].

No less complex nature is demonstrated by noise on MRI images [27]. The impact factors include the equipment parameters (like configuration of coils and scanner drifts) as well as the experiment parameters (like time to echo, time to repeat, slice thickness, flip angle, voxel volume). Besides, the signal fluctuations in a given voxel are influenced by physiological noise (like cerebral metabolism), as well as by subject's movements.

Depending on the number and configuration of the coils, the noise distribution may vary from complex Gaussian to Rice distribution. With the presence of artifacts, the distribution becomes more asymmetric, shifting towards the right tail, and is no longer described analytically [28]. A comparative analysis of literature data [27, 29, 30], as well as direct consultations with radiologists showed that the characteristic values of *PSNR* for MRI lie in the range of 10–300 in absolute terms, which roughly corresponds to 20–50 dB according to (4).

Comparing the above results, we put the following question: can individual instances of real high-tech medical images work as AE when being analyzed with the use of neural networks? The second question we set for ourselves was the following: is it possible to defend oneself against such «natural» adversarial attacks with the simplest possible means? In our investigation, we tried the defense methods proposed in [8], namely: adversarial training, Gaussian data augmentation and bounded RELU (see section 3 for a detailed description).

The rest of the paper is organized as follows. Section III describes the experimental technique, as well as the architecture of the neural network used and the simulation parameters. Section IV presents and discusses the results of the experiment. Section V formulates the conclusion on the work.

III. METODOLOGY

To answer the questions posed in Section II, we conducted a set of experiments each consisting of the following steps.

1) We train a neural network on dataset consisting of CT or, respectively, MRI images.
2) From this dataset, we select an image with $P_{\text{class source}} = 0.72$, and generate 10,000 noisy copies of this image, thereby forming a “noisy” dataset.
3) We make the classification of "noisy" dataset using a neural network trained in step 1 and calculate for it the values of $P_{\text{class result}}$
4) According to the classification results taken from the softmax layer (see expression (2)), we determine the number of elements of the “noisy” dataset, for which $P_{\text{class result}} < 0.5$.
5) We make a quantitative assessment of the similarity (distinguishability) of the source image used in step 2, and the images selected in step 4, using L_2 distance metric mentioned above:

$$L_2 = \sqrt{\sum_i \left(x_i^{'} - x_i\right)^2} \quad . \tag{5}$$

The specifics and parameters of each step are explained below.

TABLE I. NETWORK ARCHITECTURE AND PARAMETERS

Layer Type		**Input**	**Output**
Convolution + ReLU	3×3×3	0	1
Convolution + ReLU	3×3×3	1	2
Max Pooling	2×2x2	2	3
Convolution + ReLU	3×3×3	3	4
Convolution + ReLU	3×3×3	4	5
Max Pooling	2×2x2	5	6
Convolution + ReLU	3×3×3	6	7
Convolution + ReLU	3×3×3	7	8
Max Pooling	2×2x2	8	9
Convolution + ReLU	3×3×3	9	10
Convolution + ReLU	3×3×3	10	11
Max Pooling	2×2x2	11	12
Convolution + ReLU	3×3×3	12	13
Convolution + ReLU	3×3×3	13	14
UpConvolution	2×2x2	14	15
Convolution + ReLU	3×3×3	15+11	16
Convolution + ReLU	3×3×3	16	17
UpConvolution	2×2x2	17	18
Convolution + ReLU	3×3×3	18+8	19
Convolution + ReLU	3×3×3	19	20
UpConvolution	2×2x2	20	21
Convolution + ReLU	3×3×3	21+5	22
Convolution + ReLU	3×3×3	22	23
UpConvolution	2×2x2	23	24
Convolution + ReLU	3×3×3	24+2	25
Convolution	1x1x1	25	26
Softmax	2	26	27
Parameter			
Learning Rate	0.1		
Momentum	0.9		
Batch Size	128		
Epochs	32		

To configure the neural network, we used an architecture [31] that proved itself well when working with CT images of the lungs. It is a variant of convolutional network (CNN) structure combining U-Net [32] with the region proposal networks (RPN) [33]. The network parameters used are presented in Table I.

For each type of image (CT or MRI respectively), the following variants of training were used:

(a). The network is trained on source data using RELU activation function.

(b). The network is trained on source data augmented by the same images with added Gaussian noise;

(c). The network is trained on source data augmented by AE gained using FGSM and JSM attacks;

(d). The network is trained on source data, but the activation functions for the layers are replaced by Bounded ReLU.

As the source data two datasets were chosen, namely: the Lung Image Database Consortium image collection (LIDC-IDRI) [34] containing 1018 lung cancer screening thoracic CT scans and Brain MRI DataSet (BRATS 2015) [35] containing clinical imaging data of glioma patients (a total of 274 cases).

Our study was carried out using Gaussian noise, since if AE is manifested in this simple case, then it is even more possible on other, more complex noise distributions characteristic of high-tech medical images described above.

In all experiments, 8-bit images with a peak brightness of $MAX_i = 255$ were used. Gaussian noise was generated from the normal distribution with *means* = 0 and *stddev* = 0.5. These parameters correspond, on the one hand, to the characteristic values of the *PSNR* for CT and MRI working ranges justified in Section 2C, and on the other hand, to the typical *PSNR* values for image compression [36], which provide comfortable conditions for visual observation of high-tech medical images.

IV. Results and Discussion

Histograms reflecting the results of the implementation of step 4 of the methodology are shown in Fig. 4, and corresponding quantitative estimates are given in Table II.

Considering that $P_{\text{class source}} = 0.72 >> 0.5$, i.e. both "noisy" datasets were formed from a knowingly correctly recognized image, and the dispersion of superimposed noise was taken relatively small, one would expect that all elements of "noisy" datasets would be correctly recognized, i.e. $P_{\text{class result}} > 0.5$. However, the experimental results obtained (see fig. 2 as well as Table II) do not confirm this assumption. Namely, in all experiments, histograms contain elements wit $P_{\text{class result}} < 0.5$, i.e. the corresponding images are not recognized correctly. In accordance with the definition of [6], in this case, we can speak about the appearance of AE when classifying by CNN of high-tech medical images, due to the noise inherent in the technology of their formation.

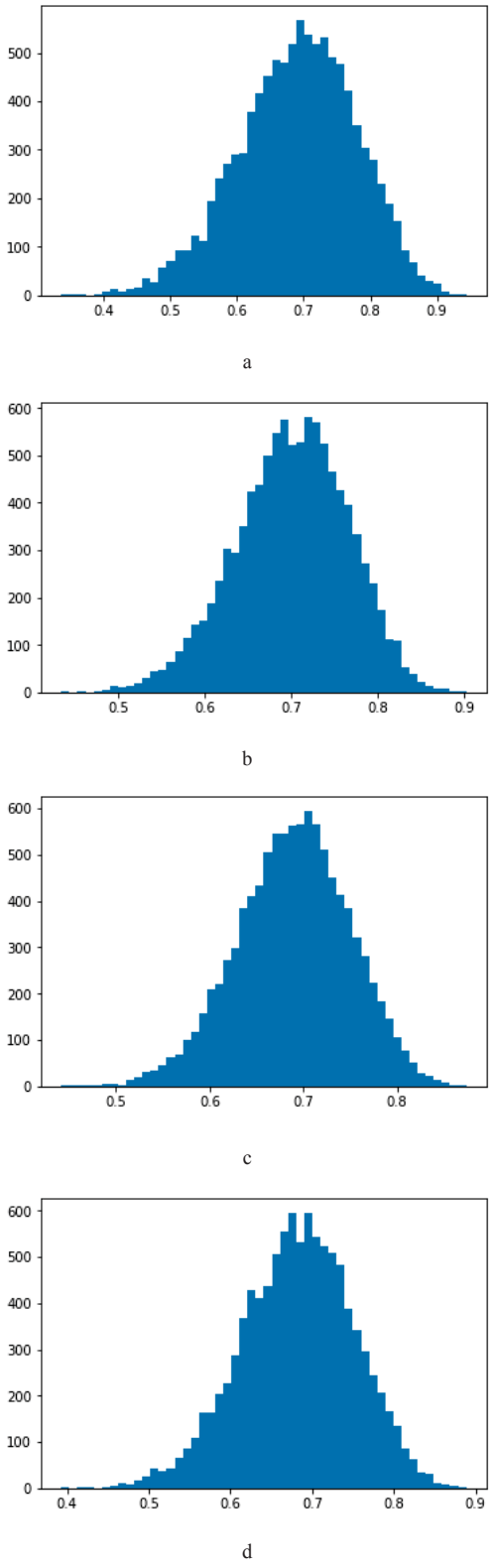

Fig. 2. Histograms of P_{class} values obtained on "noisy" dataset formed of CT image; designations of the pictures correspond to the above described network training variants (a)-(d)

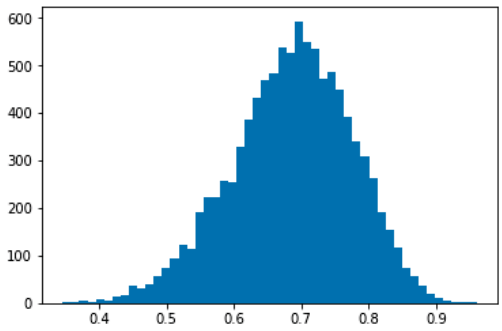

a

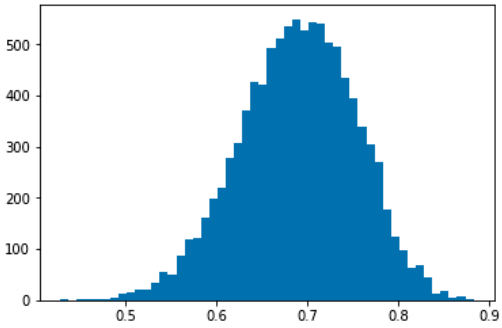

b

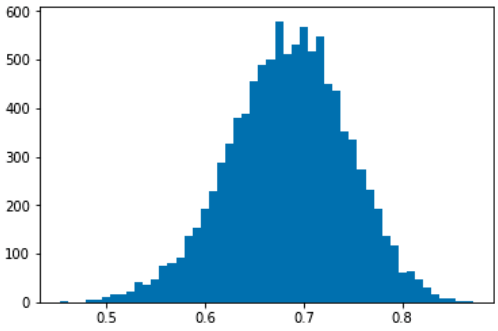

c

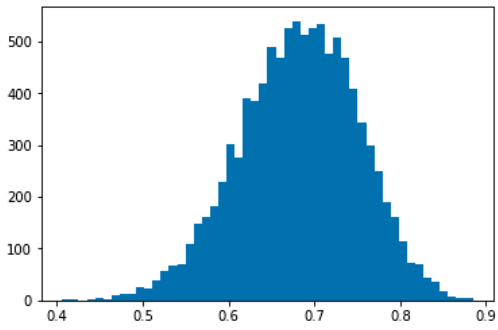

d

Fig. 3. Histograms of P_{class} values obtained on "noisy" dataset formed of MRI image; designations of the pictures correspond to the above described network training variants (a)-(d)

TABLE II. THE PROPORTION OF ELEMENTS OF THE "NOISY" DATASETS, RECOGNIZED AS INCORRECT, FOR DIFFERENT TRAINING OPTIONS

Method	Elements of "noisy" dataset with $P_{class} < 0.5$, %	
	CT	MRI
Source data	2	2.85
Source data + Gaussian data augmentation	0.21	0.26
Source data + adversarial training	0.12	0.15
Source data + Bounded RELU	0.6	0.68

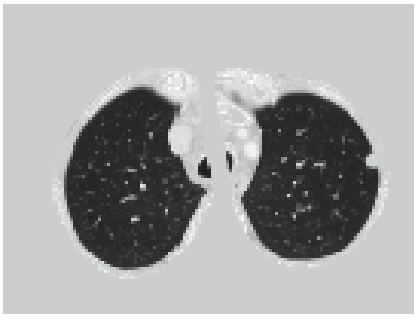

a

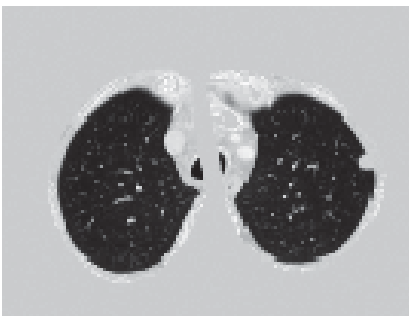

b

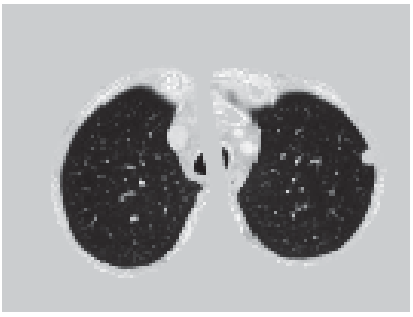

c

Fig. 4. Images of lung slices: a - source (classified by CNN as true); b - with the addition of Gaussian noise (classified by CNN as true); in - with the addition of Gaussian noise, which became AE (classified by CNN as incorrect)

Meanwhile, as shown by our experiments, the degree of manifestation of AE varies depending on the type of training model. When training a model not using techniques of defences on AE (variant (a)), the number of incorrectly recognized images is quite large (200 per 10,000 for CT and 285 per 10,000 for MRI). By proper selecting of the activation function of CNN (variant (d)), it can be reduced to 60 and 68, respectively. With augmentation of training dataset by Gaussian noised images (variant (b)), this number drops to 21

and 26, respectively. An even greater reduction in the number of incorrectly recognized images is achieved using the Adversarial Training method (variant (c)) – 12 and 15, respectively.

The results are illustrated in Fig. 3, where the real CT images of the lungs with different variants of their formation are presented. Original images were recorded in DICOM 3.0 [37] standard. To obtain our illustrations, we used the method of preprocessing DICOM data [31], which allows you to select a two-dimensional slice of the lung with cutting off other body tissues (in particular, the skeleton), and its software implementation [38]. To assess the visual similarity of the images, 3 practicing radiologists were involved.

Figures 4 and 5 show the CT images of the lungs obtained by the method described above. Fig. 4a corresponds to the original image with a value of $P_{\text{class source}} = 0.72$ (see step 2 of our methodology). In fig. 4b and 4c are shown two variants of the same image with the addition of Gaussian noise, which correspond to $P_{\text{class result}} = 0.68$ and $P_{\text{class result}} = 0.45$. The calculated value of the L_2 norm for both images was 1.89. According to experts, both images are visually identical, although one of them has become AE and will be classified by the CNN as incorrect. It can serve as a source of false information for the doctor

Fig. 5 shows a similar comparison of images obtained by CNN trained according to variant (c). In this case, the formation of AE from the original image is also possible, but this requires a significantly higher level of noise (L_2 norm increases to 4.72), and such images are easily recognized visually. Accordingly, the doctor can exclude such images from the body of diagnostic documents for a particular patient.

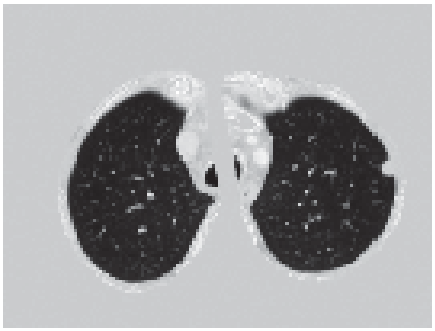

a

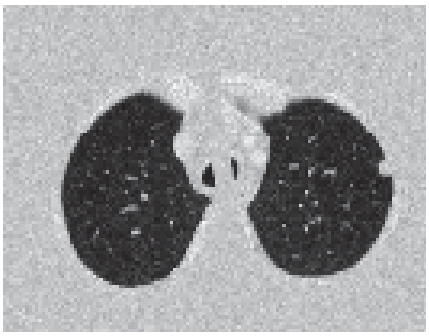

b

Fig. 5. Images of lung slices: a - source (classified by CNN as true); b - with the use of FGSM technique (classified by CNN as incorrect)

V. Conclusion

In our work, we investigated two questions: (1) can individual instances of real high-tech medical images work as AE when being analyzed with the use of CNN? (2) is it possible to defend oneself against such "natural" adversarial attacks with the simplest possible means? We answer the both formulated questions in the affirmative.

The paper shows that "natural" technological noises can become involuntary adversarial examples in high-tech medical images. A problem-oriented study of AE defense techniques (Adversarial training, Gaussian Data Augmentation, Bounded RELU) was conducted. Adversarial training techniques such as FGSM and JSM attacks have been shown to provide the best effect for high-tech medical images. It is shown that the adversarial effect is possible after the application of adversarial training techniques, but the degree of noise in such an image will be much higher than before using these techniques, and it will be easy enough for the doctor to recognize them visually and exclude them from further consideration.

Acknowledgements

This work was financially supported by Government of Russian Federation, Grant 08-08.

References

[1] Y. Ren, Y. Cao, Hu W., X. Wei, X. Shen. "Diagnostic accuracy of computed tomography imaging for the detection of differences between peripheral small cell lung cancer and peripheral non-small cell lung cancer", *Int. J. Clin. Oncol.,* Vol. 22(5), Oct. 2017, pp. 865–871. doi: 10.1007/s10147-017-1131-0.

[2] Kaggle, Data Science Bowl 2017, Web: https://www.kaggle.com/c/data-science-bowl-2017.

[3] QingZeng Song, Lei Zhao, XingKe Luo and XueChen Dou. "Using deep learning for classification of lung nodules on computed tomography images", *J Healthc Eng.*, 2017, No. 8314740. Published online 2017 Aug 9. doi: [10.1155/2017/8314740].

[4] M.F. Serj, B. Lavi, G. Hoff and D. P. Valls. "A deep convolutional neural network for lung cancer diagnostic", arXiv:1804.08170v1 [cs.CV], 22 Apr. 2018.

[5] J. Shi. "Lung nodule detection using convolutional neural networks", *Electrical Engineering and Computer Sciences University of California at Berkeley. Technical Report No. UCB/EECS-2018-27.* Web: http://www2.eecs.berkeley.edu/Pubs/TechRpts/2018/EECS-2018-27.html. May 3, 2018.

[6] C. Szegedy, W. Zaremba, I. Sutskever, J. Bruna, D. Erhan, I.J. Goodfellow and R. Fergus, "Intriguing properties of neural networks". *ICLR*, abs/1312.6199, 2014. Web: http://arxiv.org/abs/1312.6199.

[7] A. Kurakin, I.J. Goodfellow, S. Bengio, "Adversarial examples in the physical world". *Workshop track - ICLR 2017*. arXiv:1607.02533v4 [cs.CV] 11 Feb 2017

[8] V. Zantedeschi, M.-I. Nicolae, A. Rawat, "Efficient defenses against adversarial attacks". arXiv:1707.06728v2 [cs.LG] 30 Aug 2017

[9] N. Carlini, D. Wagner, "Towards evaluating the robustness of neural networks", *IEEE Symposium on Security and Privacy*, 2017. arXiv:1608.04644v2 [cs.CR] 22 Mar 2017.

[10] I. Goodfellow, J. Shlens, C. Szegedy. "Explaining and harnessing adversarial examples". *ICLR*, 2015

[11] N. Papernot, P. Mcdaniel, S. Jha, M. Fredrikson, Z.B. Celik, A. Swami. "The limitations of deep learning in adversarial settings". *1st IEEE European Symposium on Security & Privacy, IEEE 2016.* Saarbrucken, Germany. Pp. 372–387. arXiv:1511.07528v1 [cs.CR] 24 Nov 2015

[12] S.G. Finlayson, H.W. Chung, I.S. Kohane, A.L. Beam. "Adversarial attacks against medical deep learning systems", arXiv:1804.05296v2 [cs.CR] 21 May 2018

[13] T.B. Brown, D. Mane, A. Roy, M. Abadi, J. Gilmer, "Adversarial patch", arXiv:1712.09665v2 [cs.CV] 17 May 2018

[14] A. Mądry, A. Makelov, L. Schmidt, D. Tsipras, A. Vladu. "Towards deep learning models resistant to adversarial attacks". arXiv:1706.06083v3 [stat.ML] 9 Nov 2017

[15] S.A. Taghanaki, A. Das and G. Hamarneh. "Vulnerability analysis of chest X-ray image classification against adversarial attacks". 9 Jul 2018. arXiv:1807.02905

[16] W. Brendel, J. Rauber, M. Bethge, "Decision-based adversarial attacks: reliable attacks against black-box machine learning models", *ICLR 2018*. arXiv:1712.04248v2 [stat.ML] 16 Feb 2018

[17] M. Paschali, S. Conjeti, F. Navarro, N. Navab. "Generalizability vs. robustness: adversarial examples for medical imaging". arXiv:1804.00504v1 [cs.CV] 23 Mar 2018

[18] C. Xie, J. Wang, Z. Zhang, Y. Zhou, L. Xie, A.L. Yuille, "Adversarial examples for semantic segmentation and object detection". *ICCV 2017*

[19] L.J.P. van der Maaten, G.E. Hinton, "Visualizing Data Using t-SNE", *Journal of Machine Learning Research*. 2008, V. 9, pp. 2579–2605

[20] M. Diwakar, M. Kumarb. "A review on CT image noise and its denoising". *Biomedical Signal Processing and Control.* V. 42, April 2018, pp. 73–88.

[21] E.C. Ehman, L. Yu, A. Manduca, A.K. Hara, M. M. Shiung, D. Jondal, et al. "Methods for clinical evaluation of noise reduction techniques in abdominopelvic CT". *RadioGraphics* 2014, V. 34, pp. 849–862.

[22] L. Jia, Q. Zhang, Y. Shang, Y. Wang, Liu Y., N. Wang et al. "Denoising for low-dose CT image by discriminative weighted nuclear norm minimization". *IEEE Access*, V. 6, pp. 46179 – 46193. August 2018. DOI: 10.1109/ACCESS.2018.2862403

[23] W.W. Mayo-Smith, A.K. Hara, M. Mahesh, D.V. Sahani, W. Pavlicek. "How i do it: managing radiation dose in CT". *Radiology,* Vol. 273, No. 3. Nov. 2014. doi.org/10.1148/radiol.14132328

[24] G. Vegas-Sánchez-Ferrero, M.J. Ledesma-Carbayob, G.R. Washkoa, R.S.J. Estépara, "Statistical characterization of noise for spatial standardization of CT scans: Enabling comparison with multiple kernels and doses", *Med Image Anal.* 2017 August, V. 40, pp. 44–59. doi:10.1016/j.media.2017.06.001

[25] A. Chaudhari, P. Chaudhary, A.N. Cheeran, Y. Aswani. "Improving signal to noise ratio of low-dose CT image using wavelet transform". *International Journal on Computer Science and Engineering (IJCSE)*. Vol. 4, No. 05, May 2012, pp.779–787.

[26] J. Yan, J. Schaefferkoette, M. Conti, D. Townsend. "A method to assess image quality for low-dose PET: analysis of SNR, CNR, bias and image noise". *Cancer Imaging*. 2016, V.16 (1), 26. Aug. 2016. doi: 10.1186/s40644-016-0086-0

[27] D.R. Dance, S. Christofides, A.D.A. Maidment, I.D. McLean, K.H. Ng. *Diagnostic Radiology Physics. A Handbook for Teachers and Students*. IAEA, 2014. 682 p. ISBN 978–92–0–131010–1

[28] B. Mortamet, M.A. Bernstein, C.R. Jack Jr, J.L. Gunter, Ch. Ward, P.J. Britson, R. Meuli, J.-P. Thiran, G. Krueger, "Automatic quality assessment in structural brain magnetic resonance imaging". *Magn Reson Med*. 2009 August; 62(2): 365–372. doi:10.1002/mrm.21992

[29] C. Triantafyllou, J.R. Polimeni, L.L. Wald. "Physiological noise and signal-tonoise ratio in fmri with multi-channel array coils." *NeuroImage*, V. 55 (2), pp. 597–606. March 2011. doi:10.1016/j.neuroimage.2010.11.084

[30] P. Shokrollahi, J.M. Drake, A.A. Goldenberg. "Signal-to-noise ratio evaluation of magnetic resonance images in the presence of an ultrasonic motor", *Biomed Eng Online*. 2017; Vol. 16: 45. Apr. 2017. doi: 10.1186/s12938-017-0331-1

[31] F. Liao, M. Liang, Z. Li, X. Hu, S. Song, "Evaluate the malignancy of pulmonary nodules using the 3D deep leaky noisy-or network". *Journal of Latex Class Files*, Vol. 14, Nj. 8, Aug. 2015. arXiv:1711.08324v1 [cs.CV] 22 Nov 2017

[32] O. Ronneberger, P. Fischer, T. Brox. "U-net: Convolutional networks for biomedical image segmentation". *International Conference on Medical Image Computing and Computer-Assisted Intervention*. Springer, 2015, pp. 234–241.

[33] S. Ren, K. He, R. Girshick, J. Sun, "Faster R-CNN: towards real-time object detection with region proposal networks". *Advances in Neural Information Processing Systems*, 2015, pp. 91–99.

[34] lidc-dataset, Web: https://github.com/topics/lidc-dataset

[35] How to join BRATS 2015: Brain Tumor Image Segmentation Challenge. Web: https://www.virtualskeleton.ch/BRATS/Start2015

[36] STVC Video Codec. Web: https://www.sial.iias.spb.su/files/stvc.pdf

[37] DICOM Standard: Medical Imaging & Technology Alliance. Web: https://www.dicomstandard.org/current/

[38] The solution of team 'grt123' in DSB2017/ Web: https://github.com/lfz/DSB2017